

Crystallization and activation of silicon by microwave rapid annealing

Shunsuke Kimura¹ · Kosuke Ota¹ · Masahiko Hasumi¹ · Ayuta Suzuki² · Mitsuru Ushijima² · Toshiyuki Sameshima¹

Received: 15 March 2016 / Accepted: 13 June 2016
© Springer-Verlag Berlin Heidelberg 2016

Abstract A combination of the carbon-powder absorber with microwave irradiation is proposed as a rapid heat method. 2- μm -diameter carbon powders with a packing density of 0.08 effectively absorbed 2.45 GHz 1000-W-microwave and heated themselves to 1163 °C for 26 s. The present heat treatment recrystallized n-type crystalline silicon surfaces implanted with $1.0 \times 10^{15}\text{-cm}^{-2}$ -boron and phosphorus atoms with crystalline volume ratios of 0.99 and 0.93, respectively, by microwave irradiation at 1000 W for 20 s. Activation and carrier generation were simultaneously achieved with a sheet resistivity of $62\ \Omega/\text{sq}$. A high photo-induced-carrier effective lifetime of 1.0×10^{-4} s was also achieved. Typical electrical current-rectified characteristic and solar cell characteristic with an efficiency of 12.1 % under $100\text{-mW}/\text{cm}^2$ -air-mass-1.5 illumination were obtained. Moreover, heat treatment with microwave irradiation at 1000 W for 22 s successfully crystallized silicon thin films with thicknesses ranging from 2.4 to 50 nm formed on quartz substrates. Nano-crystalline cluster structure with a high volume ratio of 50 % was formed in the 1.8-nm (initial 2.4-nm)-thick silicon films. Photoluminescence around 1.77 eV was observed for the 1.8-nm-thick silicon films annealed at 260 °C in $1.3 \times 10^6\text{-Pa-H}_2\text{O}$ -vapor for 3 h after the microwave heating.

1 Introduction

We have recently proposed a simple thermal annealing method by 2.45 GHz microwave [1–5]. Incoherent microwave is effectively generated by the cavity magnetron, in which thermal electrons are accelerated under a magnetic field in the cavity resonators. The electromagnetic energy of the microwave is changed to heating energy by free carrier absorption of conductive carbon, that has low specific heat and high heat proof properties [6, 7]. To demonstrate this simple idea described above, we used a commercial 2.45 GHz microwave oven to generate microwave and used 2- μm -diameter carbon powders to cover a sample in the sample room of the oven. We observed heating of carbon powders to about 1000 °C by microwave irradiation for 120 s. We also achieved activation of silicon implanted with boron and phosphorus atoms [1, 3–5] and crystallization of 50-nm-thick silicon films formed on glass substrate [2]. Activation of silicon implanted with impurity atoms is inevitable for fabrication of devices such as metal–oxide–semiconductor field-effect transistors (MOS FETs), pn junction diodes, and solar cells [8–11]. Especially, rapid heating is important to solve the problem of the thermal budget in fabricating semiconductor devices at a low cost. A high activation ratio and no marked impurity diffusion are also attractive for fabricating an extremely shallow junction as many studies have proved [11–17]. Crystallization of amorphous silicon thin films is also important for fabricating the thin film transistors (TFTs) with a high carrier mobility and low threshold voltage, which can be applied to switching and driving circuits in flat panel displays [18–20]. It is also attractive for fabricating the thin film solar cells [21, 22]. We now focus development in the microwave heating method for fabrication processes of crystalline silicon solar cells and

✉ Toshiyuki Sameshima
tsamesim@cc.tuat.ac.jp

¹ Tokyo University of Agriculture and Technology, 2-24-16, Naka-cho, Koganei, Tokyo 184-8588, Japan

² Tokyo Electron Limited, Akasaka, Minato-ku, Tokyo 107-6325, Japan

thin film silicon solar cells. To achieve low thermal budget, rapid annealing for short heating duration is required compared with conventional hot-wall heating. Crystallization of silicon thin films with nano-meter sized crystalline grains will be important to look for quantum-well and quantum-dot types thin film solar cells. Because crystallization of silicon thin films has been not easy, heating silicon films at high temperature for a long time have been necessary [23, 24].

In this paper, we first report heating properties of carbon powders by 2.45 GHz microwave irradiation. Observation of radiation emitted from the surface of carbon powders allows real-time measurement of temperature increase. We demonstrate rapid heating with a high temperature by additional condensation optics. Next, we demonstrate activation of silicon implanted with boron and phosphorus atoms. We report the recrystallization properties of the disordered amorphous regions formed by the phosphorus and boron implantation. We also show a low sheet resistivity characteristic via activation. We then demonstrate the diode-rectified characteristics and solar cell characteristics with an efficiency of 12.1 %. Finally, we demonstrate rapid crystallization of thin silicon films by the 2.45 GHz microwave heating. Especially, we discuss crystallization behavior with Raman scattering spectra for 2.4-nm-thick silicon films.

2 Experimental procedure

A commercial microwave oven with 2.45 GHz at a microwave power of 1000 W, TOSHIBA ER-LD330, was prepared. Microwave generated by the magnetron was introduced by waveguide tubes to a dome-shaped antenna located just below the sample room. The antenna rotated with a period of 3 s to irradiate microwave uniformly to the sample room. A real-time temperature-measurement system was established with a radiation thermometer, which sensitively detected the intensity of 900-nm light radiated from hot material above 540 °C. A small hole with a diameter of 1 cm was opened at the front door of the oven to measure a temperature of samples placed in the sample room, as shown in Fig. 1a. A quartz vessel with a diameter of 3 cm was placed 2 cm above from the bottom surface of the sample room. Carbon powders with an average diameter of 2 μm and a weight of 1 g were put in the vessel. A sample to be heated was also placed in the vessel, in which the sample was covered with carbon powders, as shown in Fig. 1b. A dome-shaped metal mesh was placed above the vessel including the carbon powders and sample to reflect microwave coming from the dome antenna locating below the bottom surface and concentrate it toward the vessel, as

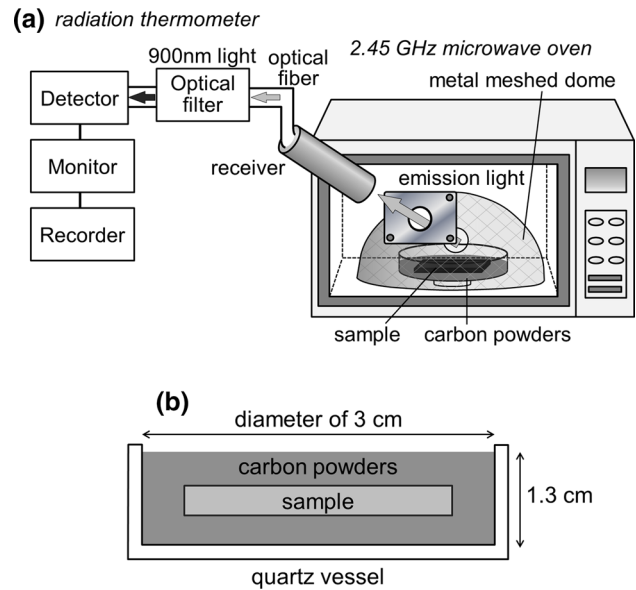


Fig. 1 **a** Schematic apparatus for a 2.45 GHz microwave heating and thermometry system. **b** Schematic image of a sample in a quartz vessel. The sample was covered with carbon powders

shown in Fig. 1a. A small hole was also opened on the metal mesh to measure temperature by the thermometer.

In advance of heat treatment, microwave absorption was estimated with different packing densities of carbon powders using the 9.35-GHz microwave transmittance measurement system [25, 26]. Quartz sheaths with a width, length, and internal gap of 3.0, 3.0, and 0.1 cm, respectively, were prepared. The sheaths were charged with carbon powders with different packing densities of 0.06, 0.08, 0.11, 0.13, 0.15, 0.18, and 0.19 determined by weight measurement. The sheath was placed in the narrow gap of waveguide tubes in the 9.35-GHz microwave-transmittance measurement system, as shown by inset in Fig. 2a. The experimental transmissivity was analyzed by a finite element numerical calculation program with a Fresnel-type microwave interference effect with refractive indexes of quartz [27] and carbon [7] and the free carrier absorption. Effective dielectric media approximation gave the refractive index of internal region of the sheath depending on the packing density of carbon powders. Best coincidence between experimental and calculated transmissivity gave the resistivity of carbon particles. The numerical calculation was also conducted with the analyzed resistivity of carbon particles in the case of a frequency of 2.45 GHz to obtain transmissivity, reflectivity, and absorptivity as a function of packing density of carbon. The highest absorptivity determined the packing density of carbon for the present heat treatment.

Ion-implanted silicon and thin silicon film samples were prepared. (1) 17- Ωcm n-type silicon substrates with a

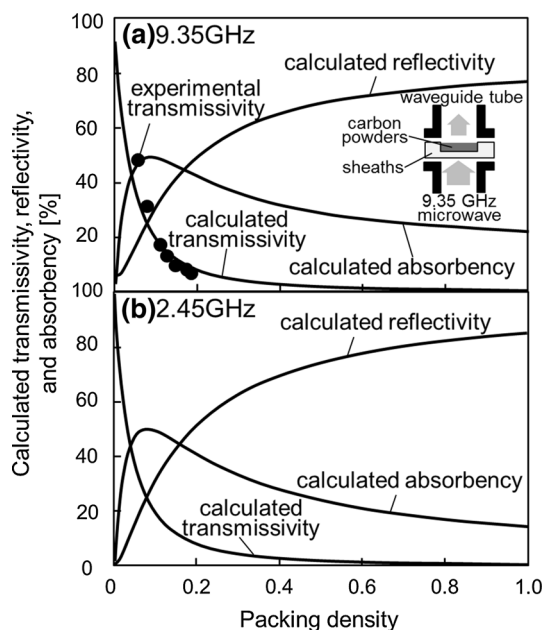


Fig. 2 **a** 9.35 GHz microwave transmissivity as a function of carbon packing density (solid circles). Solid curves show the numerically calculated transmissivity, reflectivity, and absorptivity with a conductivity of carbon powders of 0.55 S/cm as a function of carbon packing density. **b** Calculated 2.45 GHz microwave transmissivity, reflectivity, and absorptivity with a conductivity of carbon powders of 0.55 S/cm as a function of carbon packing density

thickness of 500 μm and a crystalline orientation of (100) were prepared. The silicon substrates were coated with 100-nm-thick thermally grown SiO_2 layers by heating in a wet atmosphere at 1100 $^\circ\text{C}$. The ion implantation of boron atoms was conducted for the top surface of the silicon substrates. The acceleration energy was set at 25 keV to obtain the peak concentration at the interface of the thermally grown SiO_2 and silicon. The total dose was $2.0 \times 10^{15} \text{ cm}^{-2}$. Boron atoms at a concentration of $1.0 \times 10^{15} \text{ cm}^{-2}$ were effectively implanted in the silicon substrates. The ion implantation of phosphorus atoms at 75 keV was also conducted for the rear surface of the silicon substrates. Phosphorus atoms at a concentration of $1.0 \times 10^{15} \text{ cm}^{-2}$ were effectively implanted in the silicon substrates. Most of boron and phosphorus atoms were located within 60 nm from the silicon surfaces. The sample was cut to $1.4 \times 2.4 \text{ cm}^2$ pieces. The pieces with the SiO_2 layers coated on the surfaces were subsequently heated by microwave irradiation. The SiO_2 layers prevented the incorporation of other materials such as carbon into silicon [14]. Optical reflectivity spectra were measured between 250 and 1000 nm using a conventional spectrometer to investigate the crystalline volume ratio in the ion-implanted surface regions. The spectra were analyzed using a numerical calculation program, which was constructed on

the basis of the optical interference effect for an air/multiple Si layers/Si substrate structure [28]. The most probable in-depth distribution of the crystalline volume ratio was obtained by fitting the calculated reflectivity spectra to the experimental reflectivity spectra. The SiO_2 layers were then removed by dipping the samples in 5% dilute hydrofluoric acid for 5 min. The microwave transmittances in a dark field were detected and analyzed by the finite element numerical calculation program described above to obtain the sheet resistivity. Continuous-wave (CW) 635-nm laser diode (LD) light illuminations with a light intensity of 0.74 mW/cm^2 on the sample surface were introduced. The photo-induced minority carrier effective lifetime in the cases of light illumination of the boron-implanted p^+ surface, $\tau_{\text{eff}}(p^+)$ and of the phosphorus-implanted n^+ surface, $\tau_{\text{eff}}(n^+)$ was obtained by the numerical analysis of experimental transmittances [4]. Interdigital Al electrodes were subsequently formed at the top and rear surfaces to measure electrical current as a function of bias voltage in the dark and light illuminated with Air Mass (AM) 1.5 at 100 mW/cm^2 , as shown by inset in Fig. 7. AlO_x -anti-reflection coating was then conducted by the thermally evaporation method. A sample and Al metal wire were placed in a vacuum chamber. The chamber was evacuated to $1 \times 10^{-4} \text{ Pa}$. Oxygen gas was then introduced at a gas pressure of 0.1 Pa. The Al metal wire was evaporated by current joule heating. 75-nm-thick AlO_x films with a refractive index of 1.65 were deposited on the sample surfaces via reaction of Al clusters with oxygen molecules. The samples were finally heated with $1.3 \times 10^6 \text{ Pa}$ water vapor for 3 h to decrease the defect density at the surfaces and implanted regions [29].

(2) amorphous silicon (a-Si) films with thicknesses of 2.4, 5.5, 10, 19, and 50 nm were formed on quartz substrates using plasma sputtering method. 100-nm-thick SiO_x films were subsequently formed on the surfaces of 2.4-nm-thick silicon films for preventing from evaporation of silicon during heating. The samples were then cut into $18 \times 18 \text{ mm}^2$ pieces. The samples were heated by microwave irradiation. Raman scattering spectra were measured from 400 to 600 cm^{-1} using a 514.15 nm probe laser beam and analyzed with a convolution model of crystalline, nano-crystalline, and amorphous Gaussian components to estimate the crystalline, nano-crystalline, and amorphous volume ratio. $1.3 \times 10^6 \text{ Pa-H}_2\text{O}$ vapor heat treatment at 260 $^\circ\text{C}$ was subsequently applied to the 2.4-nm-thick silicon film to reduce recombination defect states at surfaces and crystalline grain boundaries of silicon [29, 30]. Photoluminescence spectrum of the sample was measured at room temperature by 514.15-nm laser excitation with a photon energy of 2.41 eV.

3 Results and discussion

3.1 Microwave absorption by carbon powders

Figure 2a shows experimental-9.35 GHz microwave transmissivity (solid circles) of carbon powders charged in the sheaths with different packing densities, as shown in the inset. The calculated transmissivity, reflectivity, and absorbency as a function of carbon packing density were also shown by solid curves in Fig. 2a. A transmissivity of 48 % was obtained at the low carbon packing density of 0.06. The transmissivity monotonically decreased as the carbon package density increased. The best fitting calculated transmissivity to experimental ones resulted in a conductivity of carbon powders of 0.55 S/cm. The numerical calculation with 0.55 S/cm also gave reflectivity and absorbency as a function of the packing density of carbon powders. The reflectivity increased as the packing density increased because of increase in the effective extinction coefficient caused by conductivity of carbon. The peak absorbency therefore appeared at a packing density of 0.09. The numerical calculation was also conducted with the conductivity of carbon powders of 0.55 S/cm in the case of microwave frequency of 2.45 GHz, as shown in Fig. 2b. The calculated-2.45-GHz microwave transmissivity, reflectivity, and absorbency had similar characteristics to those at 9.35 GHz. The 2.45 GHz microwave absorbency had the maximum value of 50.0 % at a packing density of 0.08. For the present heat treatment, we therefore determined the packing density as 0.08, which is realized by mechanical pressing carbon powder region in the quartz vessel shown in Fig. 1b.

Figure 3 shows the change in temperature of carbon powders with time during 1000 W microwave irradiation measured by radiation thermometer. The picture in the inset of Fig. 3 shows a photo of black body bright radiation of heated carbon powders at 20 s. Carbon powders

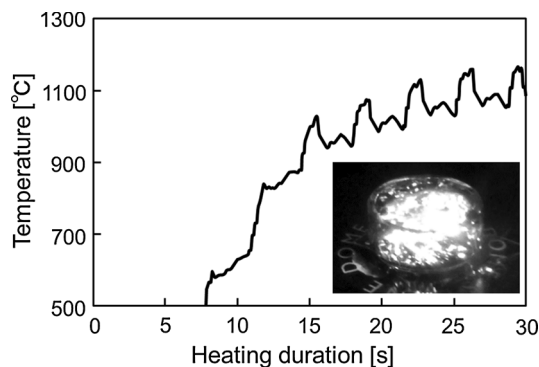


Fig. 3 Change in the temperature of carbon powders with a packing density of 0.08 during the 2.45 GHz microwave irradiation at 1000 W. The *inset* shows a photo of radiation of heated carbon powders at 20 s

effectively absorbed 2.45-GHz microwave and were rapidly heated above 1000 °C at 15 s. The temperature reached to 1163 °C at maximum at 26 s. The change in temperature showed an oscillating behavior because of the rotation with a period of 3 s and probably because the metal mesh dome did not uniformly concentrate microwave to the vessel region. The vessel was therefore irradiated with microwave periodically with high and low intensities.

3.2 Activation of implanted atoms

The optical reflectivity spectra for boron- and phosphorus-implanted n-type silicon coated with 100-nm-thick thermally grown SiO₂ layers were measured to investigate the recrystallization of impurity implanted regions by the 2.45 GHz microwave heating. Figure 4 shows optical reflectivity spectra of sample surfaces for (a) initial, as-implanted with boron and phosphorus, and (b) microwave heated for 20 s. The calculated spectra are also presented with dashed curves. The spectra included optical interference effects caused by 100-nm-thick thermally grown SiO₂ layers coated with silicon surfaces. Two large peaks of E_1 and E_2 caused by the large joint density of states at the X point in the Brillouin zone of crystalline silicon appeared at 340 and 275 nm for the initial sample. On the other hand, the peak heights of E_1 and E_2 became small for the reflectivity spectrum of boron as-implanted surface. Decreases in the heights of the peaks indicate the partial amorphization of

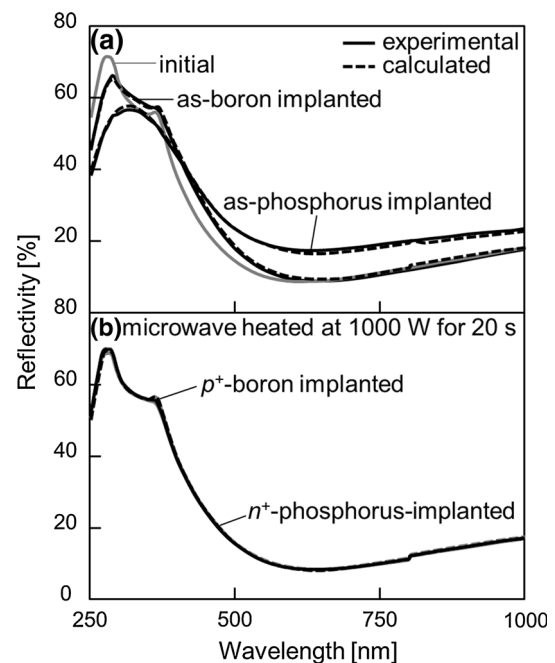


Fig. 4 Optical reflectivity spectra of sample surfaces **a** initial, as-implanted with boron and phosphorus and **b** microwave heated for 20 s. The calculated spectra are also presented with *dashed curves*

the surface region for the boron-implanted surface. Moreover, no E_1 and E_2 peaks were observed in the case of phosphorus implantation, as shown in Fig. 4a. This result indicates that the surface region was completely amorphized by the phosphorus implantation. The microwave heating for 20 s changed the optical reflectivity spectra of the boron- and phosphorus-implanted sample surfaces similar to the optical reflectivity spectrum of the initial sample having the E_1 and E_2 peaks, as shown in Fig. 4a, b. The amorphized surface regions were recrystallized by the microwave heating. Figure 4a, b also shows the numerically calculated reflectivity spectra by dashed curves, which almost coincided with the experimental ones. The best fitting process resulted in the in-depth distribution of the crystalline volume ratio for (a) boron- and (b) phosphorus-implanted surfaces, as shown in Fig. 5.

The analysis of the reflectivity spectra indicated that the boron ion implantation decreased crystalline volume ratio to 0.07 in the top 4 nm region and 0.90 from a depth of 4–50 nm because of boron implantation with a high peak concentration of $3 \times 10^{20} \text{ cm}^{-3}$. The crystalline volume ratio of surface region was increased to 0.99 by microwave heating at 1000 W for 20 s. On the other hand, the phosphorus ion implantation decreased crystalline volume ratio to 0.0 in the top 36 nm region and 0.66 from a depth of 36–39 nm as shown in Fig. 5b. The depth of amorphized region was roughly agreement with in-depth distribution of implanted boron and phosphorus atoms. The microwave heating at 1000 W for 20 s also increased crystalline

volume ratio to 0.93 in the phosphorus-implanted surface regions. These results clearly indicated that the microwave heating at 1000 W for 20 s effectively recrystallized both boron- and phosphorus-implanted surface regions.

Figure 6a shows the sheet resistivity of microwave-heated samples as a function of heating duration obtained by the analysis of the 9.35 GHz microwave transmittance measurement in a dark field. The sheet resistivity of as-implanted sample was $340 \text{ } \Omega/\text{sq}$, which was governed by majority carriers in the silicon substrate. It decreased to 62, 78, 64, and $64 \text{ } \Omega/\text{sq}$ by microwave heating at 1000 W for 20, 22, 24, and 26 s, respectively, because of the increase in carrier density in the boron- and phosphorus-implanted surface regions. The silicon substrates were sufficiently heated via the heat conduction from the hot carbon powders to move the boron and phosphorus atoms from the interstitial to the lattice sites. We achieved impurity activation by a short heating duration compared with our previous report [1]. Rapid heating was achieved by a high intensity of microwave irradiation caused by the dome-shaped metal mesh concentrating microwave toward the vessel including the sample. Figure 6b shows the $\tau_{\text{eff}}(p^+)$ and $\tau_{\text{eff}}(n^+)$ as a function of heating duration. The τ_{eff} for the initial and as-implanted samples were also presented by arrows. The initial n-type silicon substrate coated with 100-nm-thick thermally grown SiO_2 layers had a high τ_{eff} of $1.5 \times 10^{-3} \text{ s}$. Both the top and rear surfaces of silicon substrate were well passivated by the thermally grown SiO_2 layers. The τ_{eff} for boron and phosphorus as-

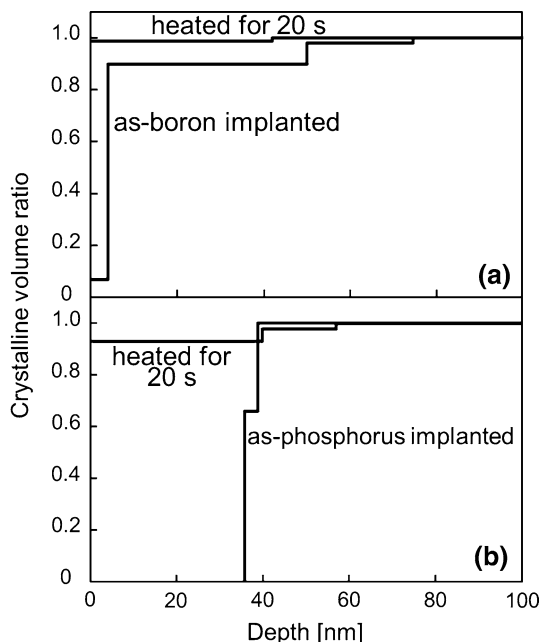


Fig. 5 In-depth distribution of crystalline volume ratio for **a** boron and **b** phosphorus-implanted surfaces in the as-implanted and microwave-heated cases analyzed from the results in Fig. 4a, b

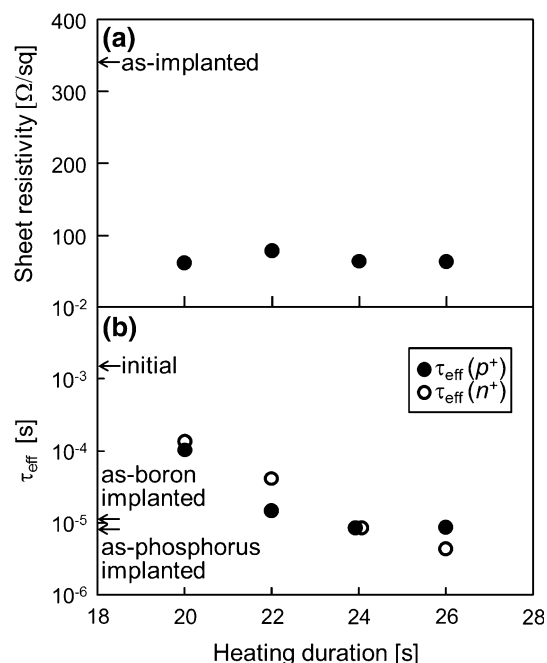


Fig. 6 Sheet resistivity **(a)** and photo-induced minority carrier effective lifetime **(b)** as a function of microwave heating duration

implanted surfaces markedly decreased to 1.2×10^{-5} and 8.3×10^{-6} s, respectively, as shown in Fig. 6b. A high density of recombination defect states were generated in the silicon surface regions by ion implantation associated with amorphization. On the other hand, the $\tau_{\text{eff}}(p^+)$ and $\tau_{\text{eff}}(n^+)$ markedly increased to 1.0×10^{-4} and 1.3×10^{-4} s, respectively, in the case of microwave heat treatment for 20 s. Those increases in $\tau_{\text{eff}}(p^+)$ and $\tau_{\text{eff}}(n^+)$ were resulted from recrystallization of the ion-implanted surface regions as well as decrease in the internal potential barrier height caused by accumulation of photo-induced carriers at the p^+ and n^+ surfaces under the condition of open circuit [4]. However, microwave heating longer than 22 s markedly decreased the $\tau_{\text{eff}}(p^+)$ and $\tau_{\text{eff}}(n^+)$. They were 8.5×10^{-6} and 4.3×10^{-6} s in the case of microwave heating for 26 s. A similar result of decrease in τ_{eff} in the case of rapid thermal annealing for the crystalline silicon coated with thermally grown SiO_2 layers in our previous report [31] suggests that stress-induced-carrier-recombination defects were seriously generated at the silicon sample surfaces in the case of microwave overheating.

Figure 7 shows logarithmic plots of absolute electrical current density as a function of applied voltage for the sample with microwave heated for 20 s under the conditions of a dark eld and AM 1.5 light illumination at 100 mW/cm^2 to the boron-implanted surface. A typical diode-rectified characteristic was observed in the dark field. The built-in potential was successfully formed by boron-implantation followed by microwave heating. The electrical current was increased exponentially by reducing the built-in potential height by forward bias voltage application. Photo-induced current and the photovoltaic effect were observed under the AM 1.5 light illumination case. The built-in potential made electron and hole currents flow in the opposite direction each other. Photo-induced

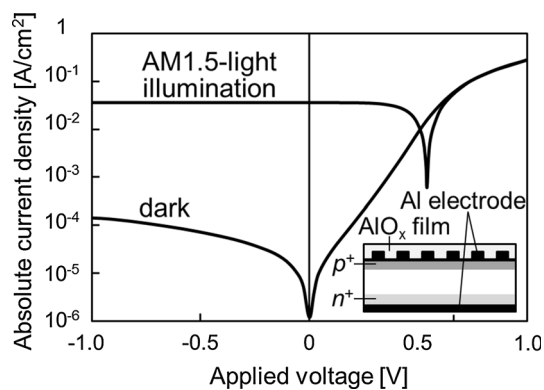


Fig. 7 Logarithmic plot of absolute-current density as a function of applied voltage for the sample with microwave heated for 20 s under the conditions of a dark eld and AM 1.5 light illumination at 100 mW/cm^2 to the boron-implanted surface

current gave a typical solar cell characteristic, as shown in Fig. 8. The short circuit current density J_{sc} , open circuit voltage V_{oc} , fill factor FF, and conversion efficiency of 35.8 mA/cm^2 , 0.54 V, 0.63, and 12.1 %, respectively. These results show that the p^+ and n^+ regions play roles of photovoltaic and back-surface-field effects [32], respectively. Figure 9 shows the conversion efficiency as a function of microwave-heating duration. The conversion efficiency was gradually decreased from 12.1 to 8.9 % as increasing the heating duration from 20 to 26 s. The decrease in the conversion efficiency was probably caused by decrease in the $\tau_{\text{eff}}(p^+)$ and $\tau_{\text{eff}}(n^+)$, as shown in Fig. 6b. The experimental results shown in Figs. 4, 5, 6, 7, 8 and 9 demonstrated the activation of silicon implanted with boron and phosphorus atoms by 2.45 GHz microwave heating at 1000 W for 20 s with carbon powders. Carbon powders effectively absorbed the microwave and the silicon samples were heated by the heat conduction. The high photo-induced carrier effective lifetime and low density of recombination defect states at the implanted regions were also achieved for 20 s microwave heating.

3.3 Crystallization of silicon thin films

The a-Si films were covered with carbon powders in the quartz vessel and heated with 2.45 GHz microwave irradiation at 1000 W for 22 s, as shown in Fig. 1a. Analyses of optical transmissivity and reflectivity revealed decrease in the film thickness by microwave heating from initial 2.4, 5.5, 10, 19, and 50 nm to 1.8, 4.2, 6.0, 18, and 49 nm, respectively, because of increase in film density via transform from amorphous to crystalline state. Figure 10 shows the Raman spectra of the initial 50-nm-thick amorphous silicon film and microwave-heated silicon films with thicknesses of 1.8, 4.2, 6.0, 18, and 49 nm measured at the central point of the samples. The initial 50-nm-thick a-Si film had a broad peak around 470 cm^{-1} associated with the

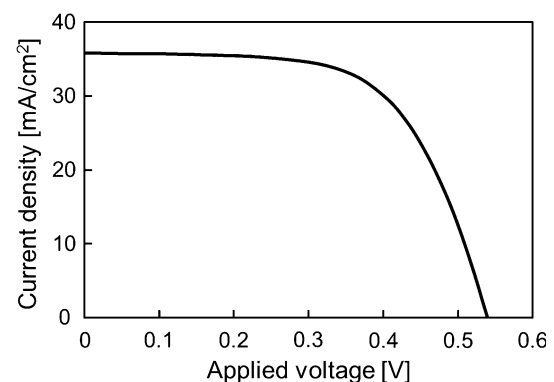


Fig. 8 Solar cell characteristics of the sample obtained from the I–V characteristics shown in Fig. 7

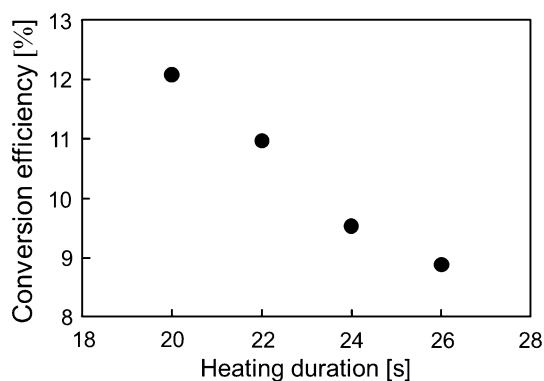


Fig. 9 Conversion efficiency as a function of microwave heating duration

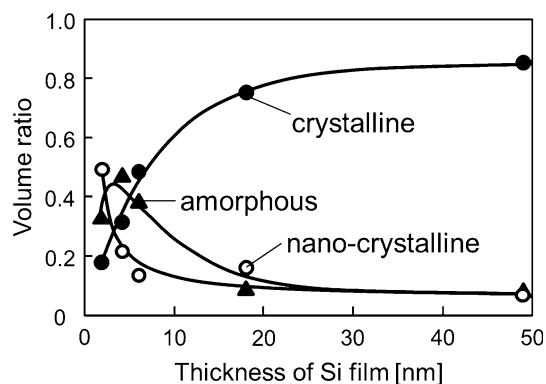


Fig. 11 Volume ratios of amorphous, nano-crystalline, and crystalline components as a function of film thickness

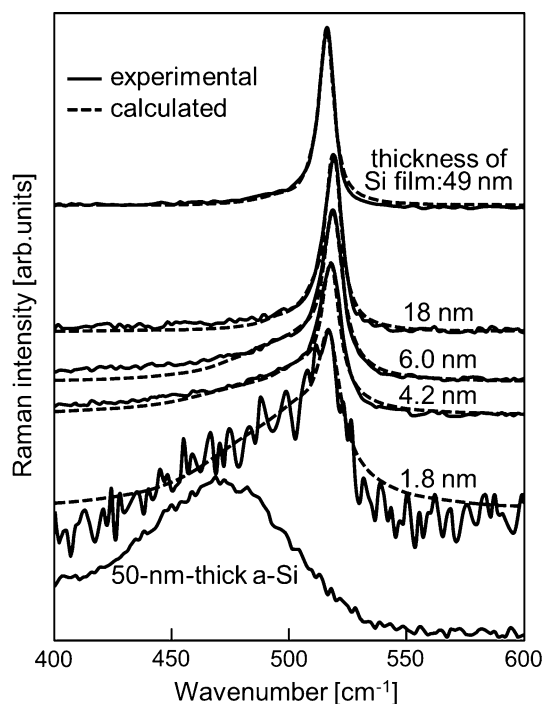


Fig. 10 Raman spectra of initial 50-nm-thick amorphous silicon film and microwave-heated a-Si films with thicknesses of 1.8, 4.2, 6.0, 18, and 49 nm

amorphous phonon mode. The other initial a-Si films with different film thicknesses showed almost the same broad spectra. On the other hand, sharp peak associated with the phonon mode of crystalline silicon appeared ranging from 515 to 518 cm^{-1} for the microwave-heated samples. Broad tail spectra associated with the phonon mode of nano-crystalline structure were also observed at around 500 cm^{-1} in the case of 1.8-nm-thick silicon film. Analysis of the spectra with three Gaussian components resulted in the volume ratios of amorphous, nano-crystalline, and crystalline regions each film thickness as shown in Fig. 11. The crystalline volume ratio increased from 0.18 to 0.85 as

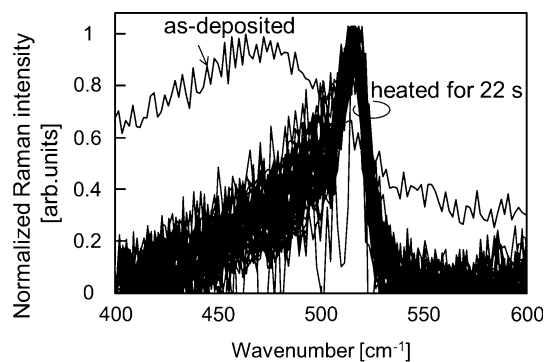


Fig. 12 Raman spectra at 36 points by a 3-mm step over the $18 \times 18 \text{ mm}^2$ for the 1.8-nm-thick-microwave-heated sample. Raman spectrum for the initial-as-deposited-2.4-nm-thick amorphous silicon film is also presented

film thickness increased from 1.8 to 49 nm. A high crystalline volume ratio was obtained for thicknesses above 20 nm. On the other hand, it is interesting that the nano-crystalline volume ratio dominated to be 0.49 at the film thickness of 1.8 nm. This analysis suggests that localized crystalline clusters with the highly-damping-type phonon mode were formed by microwave heating at 1000 W for 22 s. Large crystalline grain growth was limited by a thin film thickness. Raman spectra were measured at 36 points by a 3-mm step over the $18 \times 18 \text{ mm}^2$ for the 1.8-nm-thick-microwave-heated sample, as shown in Fig. 12. A broad Raman spectrum for the initial-2.4-nm-thick silicon film sample was also presented for comparison. Similar spectra including crystalline, nano, and amorphous phonon modes were observed all of the points. Nano-crystalline structural formation was well achieved over a whole area the 1.8-nm-thick silicon film by the microwave heat treatment for 22 s.

Figure 13 shows the 514.15-nm-laser-excited photoluminescence spectrum of 1.8-nm (initial 2.4-nm)-thick silicon film microwave heated at 1000 W for 22 s and then annealed in $1.3 \times 10^6 \text{ Pa-H}_2\text{O}$ vapor at 260 $^\circ\text{C}$ for 3 h. An

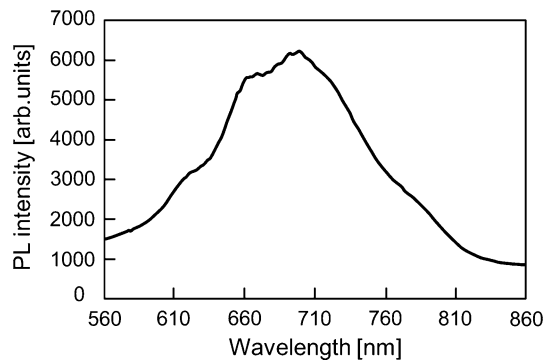


Fig. 13 514.15-nm-laser-excited photoluminescence spectrum for the 1.8-nm (initial 2.4-nm)-thick silicon film microwave heated at 1000 W for 22 s followed by annealed in 1.3×10^6 -Pa- H_2O vapor at 260 °C for 3 h

important luminescence broad peak was observed in wavelength around 700 nm (photon energy of 1.77 eV) associated with nano-crystalline silicon grains [33], which changed the indirect band structure with a band gap of 1.12 eV and allowed photo emission by the direct transition between higher energy levels.

4 Conclusions

We reported heating properties of carbon powders by 2.45-GHz microwave irradiation and its application to activation of silicon implanted with impurity atoms and to crystallization of amorphous silicon thin films. Observation of blackbody radiation revealed that 2- μm -diameter carbon powders with a packing density of 0.08 were heated to 1163 °C by 1000-W-microwave irradiation for 26 s. The present heat treatment of a combination of the carbon-powder absorber with microwave irradiation at 1000 W for 20 s successfully achieved four important results for n-type crystalline silicon with implanted surfaces with $1.0 \times 10^{15}\text{-cm}^{-2}$ -boron at 25 keV and $1.0 \times 10^{15}\text{-cm}^{-2}$ -phosphorus at 75 keV. (1) The crystalline volume ratio increased to 0.99 and 0.93 at boron- and phosphorus-implanted surfaces, respectively. (2) The sheet resistivity decreased from 340 (initial) to 62 Ω/sq , in which activation and carrier generation in the boron- and phosphorus-implanted regions contributed. (3) The photo-induced carrier effective lifetime markedly increased to 1.0×10^{-4} s because of recrystallization and carrier generation in the implanted regions. (4) Typical electrical-current-rectified characteristic and solar cell characteristic with an efficiency of 12.1 % under 100 mW/cm² AM 1.5 illumination were obtained. Moreover, the present heat treatment with microwave at 1000 W for 22 s successfully crystallized silicon thin films with thicknesses ranging from 2.4 to 50

nm formed on quartz substrates. Nano-crystalline-cluster structures with a high volume ratio of 50 % were also formed in the 1.8-nm (initial 2.4-nm)-thick silicon films. Photo luminescence was observed in wavelength around 700 nm by 515.14-nm laser excitation for the 1.8-nm-thick silicon film annealed at 260 °C in 1.3×10^6 -Pa- H_2O vapor for 3 h after the microwave heating. It was probably attributable to the direct energy transition in nano-silicon-cluster. Those results indicate that the present heat treatment has a possibility of application of silicon bulk and quantum-dot-type solar cells.

Acknowledgments This work was partly supported by Grants-in-Aid for Scientific Research C (No. 25420282) from the Ministry of Education, Culture, Sports, Science and Technology of Japan, Japan Science and Technology Agency A-STEP (No. AS2621088J), and Sameken Co., Ltd.

References

1. M. Hasumi, T. Nakamura, S. Yoshidomi, T. Sameshima, *Jpn. J. Appl. Phys.* **53**, 05FV05-1-6 (2014)
2. T. Nakamura, S. Yoshidomi, M. Hasumi, T. Sameshima, T. Mizuno, *Mater. Res. Soc. Symp. Proc.* **1666**, A13-09 (2014)
3. T. Sameshima, T. Nakamura, S. Yoshidomi, M. Hasumi, T. Ishii, Y. Inouchi, M. Naito, T. Mizuno, *International Conference on Solid State Devices and Materials*, Hilton Fukuoka Sea Hawk, Japan, 24–27 Sep 2013
4. T. Sameshima, T. Motoki, K. Yasuda, T. Nakamura, M. Hasumi, T. Mizuno, *Jpn. J. Appl. Phys.* **54**, 081302-1-6 (2015)
5. S. Kimura, M. Hasumi, K. Ota, T. Sameshima, *International Conference on Solid State Devices and Materials*, C-7-6 (2015)
6. M. Yoshikawa, N. Nagai, M. Matsuki, H. Fukada, G. Katagiri, H. Ishida, A. Ishitani, I. Nagai, *Phys. Rev. B* **46**, 7169 (1992)
7. T. Sameshima, N. Andoh, *Jpn. J. Appl. Phys.* **44**, 7305–7308 (2005)
8. S.M. Sze, *Semiconductor Devices* (Wiley, New York, 1985)
9. M. Mehrotra, J.C. Hu, A. Jain, W. Shiau, V. Reddy, S. Aur, M. Rodder, *Electron Devices Meeting. IEDM '99. Technical Digest. International, IEEE, Washington, DC, USA, 5–8 Dec 1999*. doi:10.1109/IEDM.1999.824183
10. T. Ito, K. Sugano, M. Tamura, T. Taniguchi, Y. Ushiku, T. Iinuma, T. Itani, M. Yoshioka, T. Owada, Y. Imaoka, H. Murayama, T. Kusuda, *Ext. Abstr. 3rd International Workshop Junction Technology*, p. 23 (2002)
11. A. Shima, A. Hiraiwa, *Jpn. J. Appl. Phys.* **45**, 5708 (2006)
12. R.F. Wood, C.E. Giles, *Phys. Rev. B* **23**, 2923 (1981)
13. T. Sameshima, S. Usui, M. Sekiya, *J. Appl. Phys.* **62**, 711 (1987)
14. T. Sameshima, M. Maki, M. Takiuchi, N. Andoh, N. Sano, Y. Matsuda, Y. Andoh, *Jpn. J. Appl. Phys.* **46**, 6474 (2007)
15. K. Matsumoto, A. Ohta, S. Miyazaki, S. Higashi, *Jpn. J. Appl. Phys.* **50**, 04DA07 (2011)
16. P. Kohli, S. Ganguly, T. Kirichenko, H.J. Li, S. Banerjee, E. Graetz, M. Shevelev, *J. Electron. Mater.* **31**, 214 (2002)
17. K. Ukawa, Y. Kanda, T. Sameshima, N. Sano, N. Hamamoto, *Jpn. J. Appl. Phys.* **49**, 076503 (2010)
18. T. Sameshima, K. Kogure, S. Yoshidomi, T. Haba, M. Hasumi, N. Sano, *J. Laser Micro/Nanoeng.* **4**, 227 (2009)
19. T. Sameshima, N. Andoh, *Matter. Res. Soc. Symp. Proc.* **849**, KK9.5 (2004)

20. S.C. Fong, C.Y. Wang, T.H. Chang, T.S. Chin, *Appl. Phys. Lett.* **94**, 102104 (2009)
21. P. Xu, C. Fu, C. Hu, D.W. Zhang, D. Wu, J. Luo, C. Zhao, Z. Zhang, S. Zhang, *Appl. Phys. Lett.* **102**, 122114 (2013)
22. M. Hasumi, J. Takenezawa, T. Nagao, T. Sameshima, *Jpn. J. Appl. Phys.* **50**, 03CA03 (2011)
23. S. Yamada, Y. Kurokawa, S. Miyajima, M. Konagai, *Nanoscale Res. Lett.* **9**(1), 246 (2014)
24. G.F. Grom, D.J. Lockwood, J.P. McCaffrey, H.J. Labb, P.M. Fauchet, B. White Jr., J. Diener, D. Kovalev, F. Koch, L. Tsybeskov, *Nature* **407**, 358–361 (2000)
25. T. Sameshima, H. Hayasaka, T. Haba, *Jpn. J. Appl. Phys.* **48**, 021204 (2009)
26. T. Sameshima, R. Ebina, K. Betsuin, Y. Takiguchi, M. Hasumi, *Jpn. J. Appl. Phys.* **52**, 011801 (2013)
27. E.D. Palk, *Handbook of Optical Constants of Solids* (Academic Press, London, 1985), p. 547
28. T. Sameshima, N. Andoh, Y. Andoh, *Jpn. J. Appl. Phys.* **44**, 1186–1191 (2005)
29. T. Sameshima, M. Satoh, *Jpn. J. Appl. Phys.* **36**, L687–L689 (1997)
30. T. Sameshima, H. Hayasaka, M. Maki, A. Masuda, T. Matsui, M. Kondo, *Jpn. J. Appl. Phys.* **46**, 1286–1289 (2007)
31. T. Sameshima, S. Shibata, *Jpn. J. Appl. Phys.* **53**, 061301-1-6 (2014)
32. S. Narasimha, A. Rohatgi, A.W. Weeber, *I.E.E.E. Trans, Electron Dev.* **60**, 1363 (1999)
33. M.D. Mason, G.M. Credo, K.D. Weston, S.K. Buratto, *Phys. Rev. Lett.* **80**, 5405 (1998)